

Vibrationally resonant imaging of a single living cell by supercontinuum-based multiplex coherent anti-Stokes Raman scattering microspectroscopy

Hideaki Kano and Hiro-o Hamaguchi

Department of Chemistry, The University of Tokyo, Hongo 7-3-1, Bunkyo, Tokyo 113-0033, JAPAN
hkano@chem.s.u-tokyo.ac.jp

Abstract: Supercontinuum-based multiplex coherent anti-Stokes Raman scattering (CARS) microspectroscopy has been applied to vibrational imaging of a living fission yeast cell. We have successfully extracted only a vibrationally resonant CARS image from a characteristic spectral profile in the C-H stretching vibrational region. Using our simple but sensitive analysis, the vibrational contrast is significantly improved in comparison with a CARS imaging at a fixed Raman shift. The CARS image of a living yeast cell indicates several areas at which the signal is remarkably strong. They are considered to arise from mitochondria.

©2005 Optical Society of America

OCIS codes: (300.6230) Spectroscopy, coherent anti-Stokes Raman scattering; (110.0180) Microscopy; (190.4370) Nonlinear optics, fibers

References and links

1. A. Zumbusch, G. R. Holtom, and X. S. Xie, "Three-dimensional vibrational imaging by coherent anti-Stokes Raman scattering," *Phys. Rev. Lett.* **82**, 4142-4145 (1999).
2. M. Hashimoto, T. Araki, and S. Kawata, "Molecular vibration imaging in the fingerprint region by use of coherent anti-Stokes Raman scattering microscopy with a collinear configuration," *Opt. Lett.* **25**, 1768-1770 (2000).
3. J.-X. Cheng, Y. K. Jia, G. Zheng, and X. S. Xie, "Laser-scanning coherent anti-Stokes Raman scattering microscopy and applications to cell biology," *Biophys. J.* **83**, 502-509 (2002).
4. M. Müller and J. M. Schins, "Imaging the thermodynamic state of lipid membranes with multiplex CARS microscopy," *J. Phys. Chem. B* **106**, 3715-3723 (2002).
5. H. N. Paulsen, K. M. Hilligsoe, J. Thogersen, S. R. Keiding, and J. J. Larsen, "Coherent anti-Stokes Raman scattering microscopy with a photonic crystal fiber based light source," *Opt. Lett.* **28**, 1123-1125 (2003).
6. T. Ichimura, N. Hayazawa, M. Hashimoto, Y. Inouye, and S. Kawata, "Tip-enhanced coherent anti-Stokes Raman scattering for vibrational nanoimaging," *Phys. Rev. Lett.* **92**, 220801-220804 (2004).
7. J.-X. Cheng and X. S. Xie, "Coherent anti-Stokes Raman scattering microscopy: instrumentation, theory, and applications," *J. Phys. Chem. B* **108**, 827-840 (2004).
8. H. Kano and H. Hamaguchi, "Near-infrared coherent anti-Stokes Raman scattering microscopy using supercontinuum generated from a photonic crystal fiber," *Appl. Phys. B* **B80**, 243-246 (2005).
9. J.-X. Cheng, L. D. Book, and X. S. Xie, "Polarization coherent anti-Stokes Raman scattering microscopy," *Opt. Lett.* **26**, 1341-1343 (2001).
10. A. Volkmer, L. D. Book, and X. S. Xie, "Time-resolved coherent anti-Stokes Raman scattering microscopy: imaging based on Raman free induction decay," *Appl. Phys. Lett.* **80**, 1505-1507 (2002).
11. G. W. H. Wurpel, J. M. Schins, and M. Müller, "Chemical specificity in three-dimensional imaging with multiplex coherent anti-Stokes Raman scattering microscopy," *Opt. Lett.* **27**, 1093-1095 (2002).
12. C. Otto, A. Voroshilov, S. G. Kruglik, and J. Greve, "Vibrational bands of luminescent zinc(II)-octaethylporphyrin using a polarization-sensitive "microscopic" multiplex CARS technique," *J. Raman Spectrosc.* **32**, 495-501 (2001).
13. J.-X. Cheng, A. Volkmer, L. D. Book, and X. S. Xie, "Multiplex coherent anti-Stokes Raman scattering microspectroscopy and study of lipid vesicles," *J. Phys. Chem. B* **106**, 8493-8498 (2002).
14. C. L. Evans, E. O. Potma, and X. S. Xie, "Coherent anti-Stokes Raman scattering spectral interferometry: determination of the real and imaginary components of nonlinear susceptibility $\chi^{(3)}$ for vibrational microscopy," *Opt. Lett.* **29**, 2923-2925 (2004).
15. T. W. Kee and M. T. Cicerone, "Simple approach to one-laser, broadband coherent anti-Stokes Raman scattering microscopy," *Opt. Lett.* **29**, 2701-2703 (2004).

16. H. Kano and H. Hamaguchi, "Ultrabroadband ($>2500\text{ cm}^{-1}$) multiplex coherent anti-Stokes Raman scattering microspectroscopy using a supercontinuum generated from a photonic crystal fiber," *Appl. Phys. Lett.* (accepted).
17. J. K. Ranka, R. S. Windeler, and A. J. Stentz, "Visible continuum generation in air-silica microstructure optical fibers with anomalous dispersion at 800 nm," *Opt. Lett.* **25**, 25-27 (2000).
18. M. L. Hu, C. Y. Wang, L. Chai, and A. M. Zheltikov "Frequency-tunable anti-Stokes line emission by eigenmodes of a birefringent microstructure fiber," *Opt. Exp.* **12**, 1932-1937 (2004), <http://www.opticsexpress.org/abstract.cfm?URI=OPEX-12-9-1932>.
19. M. L. Hu, C. Y. Wang, Y. Li, Z. Wang, L. Chai, and A. M. Zheltikov "Multiplex frequency conversion of unamplified 30-fs Ti: sapphire laser pulses by an array of waveguiding wires in a random-hole microstructure fiber," *Opt. Exp.* **12**, 6129-6134 (2004), <http://www.opticsexpress.org/abstract.cfm?URI=OPEX-12-25-6129>.
20. H. Kano and H. Hamaguchi, "Characterization of a supercontinuum generated from a photonic crystal fiber and its application to coherent Raman spectroscopy," *Opt. Lett.* **28**, 2360-2362 (2003).
21. H. Kano and H. Hamaguchi, "Femtosecond coherent anti-Stokes Raman scattering spectroscopy using a supercontinuum generated from a photonic crystal fiber," *Appl. Phys. Lett.* **85**, 4298-4300 (2004).
22. T. Nagahara, K. Imura, and H. Okamoto, "Time-resolved scanning near-field optical microscopy with supercontinuum light pulses generated in microstructure fiber," *Rev. Sci. Instrum.* **75**, 4528-4533 (2004).
23. R. Holzwarth, T. Udem, T. W. Hänsch, J. C. Knight, W. J. Wadsworth, and P. S. J. Russell, "Optical frequency synthesizer for precision spectroscopy," *Phys. Rev. Lett.* **85**, 2264-2267 (2000).
24. A. Volkmer, J.-X. Cheng, and X. S. Xie, "Vibrational imaging with high sensitivity via epidetecting coherent anti-Stokes Raman scattering microscopy," *Phys. Rev. Lett.* **87**, 023901-023904 (2001).
25. G. W. H. Wurpel, J. M. Schins, and M. Müller, "Direct measurement of chain order in single phospholipid mono- and bilayers with multiplex CARS," *J. Phys. Chem. B* **108**, 3400-3403 (2004).
26. Y.-S. Huang, T. Karashima, M. Yamamoto, and H. Hamaguchi, "Molecular-level pursuit of yeast mitosis by time- and space-resolved Raman spectroscopy," *J. Raman Spectrosc.* **34**, 1-3 (2003).
27. Y.-S. Huang, T. Karashima, M. Yamamoto, T. Ogura, and H. Hamaguchi, "Raman spectroscopic signature of life in a living yeast cell," *J. Raman Spectrosc.* **35**, 525-526 (2004).

1. Introduction

Coherent anti-Stokes Raman scattering (CARS) microscopy has become a powerful technique for three-dimensional vibrational imaging of chemical and biological samples [1-8]. Recently, significant progress has been made of CARS microscopy such as near-infrared excitation [1], epi-detection [9], time-resolved detection [10], multiplex measurement [11-13], and heterodyne detection [14]. Among them, multiplex CARS microspectroscopy is especially useful because it is capable of obtaining not only a CARS image but also CARS spectrum with a data-acquisition time faster than conventional spontaneous Raman microscopy. Recently, the spectral coverage of the multiplex CARS detection has been significantly broadened using a supercontinuum Stokes laser, which has been reported independently by Kee and Cicerone [15] and by us [16]. In these setups, supercontinuum is generated from a tapered fiber [15] or a photonic crystal fiber (PCF) [16] using a femtosecond Ti:Sapphire oscillator. Owing to a low threshold of the continuum generation [5, 17-19], various kinds of applications such as spectroscopy [20-22] and metrology [23] have been reported only using a single Ti: Sapphire oscillator. It is also advantageous in microscopy because many studies on CARS microscopy require a complicated laser system such as an amplified laser source or two-synchronized oscillators. Using the supercontinuum as the ultrabroadband Stokes laser, ultrabroadband multiplex CARS microspectroscopy has been demonstrated over a 2500cm^{-1} -wavenumber region, which spans from the fingerprint region to the C-H or O-H stretching region [15, 16].

It is well known that the vibrationally resonant CARS signal is often overwhelmed by a nonresonant background, which results in degradation of the vibrational contrast of a CARS image [7]. Several reports have been made of the suppression of the nonresonant background using the polarization-sensitive detection [9], epi-detection [24], time-resolved detection [10], and heterodyne detection [14]. However, some techniques decrease the resonant CARS signal itself [9, 10], and the other requires complicated experimental setup for a local oscillator [14]. In the present study, we have applied ultrabroadband multiplex CARS microspectroscopy to a living yeast cell, and succeeded in obtaining a resonant CARS image with significantly enhanced vibrational contrast. Instead of employing complicated setup, we analyzed carefully

the CARS spectral profile, and extracted only the resonant component. The key is an interference of the resonant CARS signal with the nonresonant background, which works as a local oscillator for the resonant CARS signal [25].

2. Experimental

The ultrabroadband multiplex CARS microspectroscopy using a PCF is described elsewhere [16]. Briefly, an unamplified mode-locked Ti:Sapphire laser (Coherent, Vitesse-800) was used as a laser source. Typical duration, pulse energy, peak wavelength, and repetition rate were 100 fs, 12 nJ, 801 nm, and 80 MHz, respectively. A portion of the output from the oscillator was used for a seed laser to generate a supercontinuum in the PCF (Crystal Fibre, NL-PM-750). The fundamental of the Ti:Sapphire laser and the supercontinuum were used for the pump (ω_1) and Stokes (ω_2) lasers, respectively. In order to obtain CARS spectrum with high frequency resolution, the pump laser pulses were spectrally filtered using a narrow-bandpass filter. The peak position and bandwidth were measured to be about 12490 cm^{-1} (800.6 nm) and 23 cm^{-1} , respectively. For Raman resonance, the wavelength of the Stokes laser must be in the near-infrared (NIR) region because that of the pump laser is also in the NIR. The visible component in the supercontinuum was thereby blocked by a long-wavelength-pass filter. The pulse energy of the pump and Stokes lasers were 120 and 140 pJ, respectively. Two laser pulses were superimposed collinearly using an 800-nm Notch filter, and then tightly focused onto the sample with a 40×0.9 NA microscope objective. We used an inverted microscope (Nikon, TE2000-S), which was modified for our setup. The forward-propagating CARS signal was collected with a 40×0.6 NA microscope objective. After passing through 800-nm Notch and short-wavelength-pass filter, the CARS signal was spectrally dispersed by a polychromator (Acton, SpectraPro-300i) and detected by a CCD camera (Roper Scientific, Spec-10:400BR/XTE). The sample was scanned by a piezo stage (MadCity, Nano-LP-100) with a step size of 153 nm in both the x and y directions. An exposure time for each point was 200 ms. The lateral and axial spatial resolutions in the present setup were $0.59\pm 0.01\text{ }\mu\text{m}$ and $4.2\pm 0.3\text{ }\mu\text{m}$, respectively. We used fission yeast *Schizosaccharomyces pombe* (*S. pombe*) as a sample [26, 27]. Yeast cells in water were spread on a slide-glass and sandwiched with a cover-glass. Because of a small quantity of the sample, yeast cells were immobilized between a slide-glass and a cover-glass. All measurements were performed at room temperature.

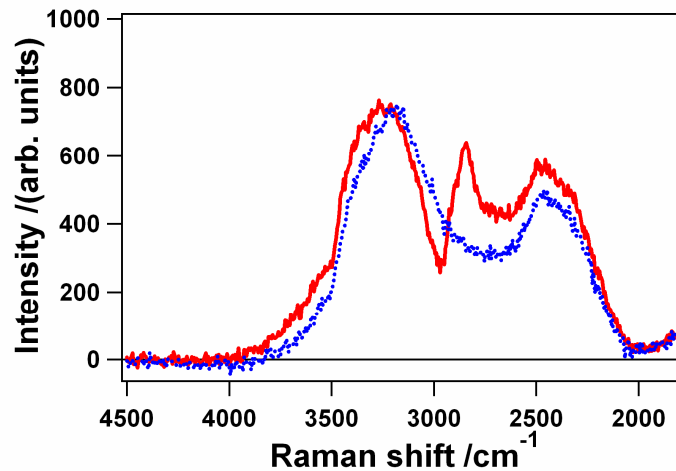


Fig. 1. Typical spectral profile of the CARS signal of a living yeast cell (red solid) and surrounding water (blue dotted)

3. Results and discussion

Typical spectral profiles of the CARS signal from a living yeast cell and surrounding water are shown in Fig. 1. The overall CARS spectral profile depends on the temporal overlap between the pump and Stokes laser pulses, because the supercontinuum Stokes pulses are temporally chirped due to a fiber dispersion [16]. By changing the delay time between the pump and Stokes laser pulses, we can control the spectral coverage of the CARS measurement and a wavenumber region at which the CARS signal is obtained with high detection efficiency. In the present setup, the delay time is optimized for efficient detection of the CARS signal due to the C-H stretching vibrational mode. As clearly shown in Fig. 1, a dispersive lineshape is observed around 2856 cm^{-1} , which is due to an interference of the resonant C-H stretching CARS signal with the nonresonant background. Because of this interference, the resonant CARS signal is intrinsically heterodyne-detected by the nonresonant background. On the other hand, the vibrationally nonresonant background signal of water shows a featureless spectral profile that represents that of the supercontinuum. Figure 2(a) and (b) shows the CARS images of living yeast cells at the Raman shift of 2856 cm^{-1} and 2200 cm^{-1} , respectively. It is noted that both images are simultaneously obtained by the multiplex CARS detection. The CARS spectra of a yeast cell (red solid) and water background (blue dotted) in Fig. 1 are obtained at $(x, y) = (-1.98\text{ }\mu\text{m}, -1.37\text{ }\mu\text{m})$ and $(-3.05\text{ }\mu\text{m}, 3.05\text{ }\mu\text{m})$ positions, which are indicated as black and white crosses in Fig. 2(a), respectively. At 2856 cm^{-1} , the resonant CARS signal is observed mainly from yeast cells, although the vibrational contrast is degraded due to the nonresonant background surrounding the cells. The dark and round region around the center of the yeast cell is most probably due to a nucleus. On the other hand, the contrast is dramatically decreased in Fig. 2(b) because there is no vibrational resonance at this Raman shift. Both in Fig 2(a) and (b), an outline of a yeast cell is observed as a dark region. The observed pattern is caused by a distortion of the focus spots due to refractive index mismatch [7].

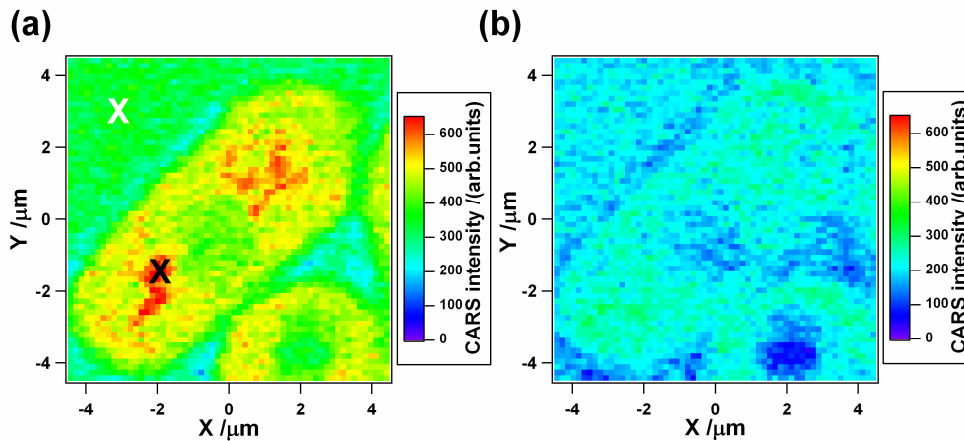


Fig. 2. CARS lateral images of living yeast cells at the Raman shift of 2856 cm^{-1} (a) and 2200 cm^{-1} (b). The black and white crosses in (a) correspond to the positions at which the spectral profiles are shown in Fig. 1.

In order to avoid the degradation due to the nonresonant background and to increase the vibrational contrast, we need to extract only the resonant CARS signal intensity. In order to separate the resonant and nonresonant CARS signal, it is useful to analyze the spectral profile of the CARS signal. As discussed in Fig. 1, the CARS spectrum has a dispersive lineshape due to the interference between the resonant and nonresonant components. The dispersive lineshape can be regarded as a characteristic and meaningful spectral pattern because the

CARS signal at water gives no such a noticeable profile. Therefore, we differentiate the CARS spectral profile at each position in order to enhance the dispersive spectral profile. If this analysis gives a large value at the peak of the differentiated spectral profile, it indicates that a chemical compound with a particular chemical bond such as a C-H bond is rich in that position. Figure 3(a) shows a result of the resonant CARS imaging using our derivative method. The original data is the same as that in Fig. 2. A detailed procedure to extract the resonant component is in the following. First, the spectral profile at each point is fitted by a third-order polynomial function in the range from 2770 to 3080 cm^{-1} . Second, the fitted curve is differentiated. Finally, the value at the peak position of the differentiated curve is mapped. A small offset value from water has been subtracted. As clearly observed, the vibrational contrast is significantly improved in comparison with Fig 2, which is a CARS image at a particular Raman shift. It is emphasized that this procedure cannot be performed with a single-wavenumber detection, because the analysis in the present study needs spectral information. As shown in Fig. 3(a), an overall flat intensity distribution is mainly observed in a yeast cell. There are various kinds of compounds in a yeast cell such as proteins, lipids, and saccharides, all of which give C-H stretching Raman resonances. Therefore, the flat offset observed in a yeast cell is assigned to those chemical compounds. On the other hand, there are several areas at which the resonant CARS signal is particularly strong. Taking account of our previous Raman studies [26, 27], it is ascribed to mitochondria, because mitochondrion is an organelle containing a high concentration of phospholipids. This assignment agrees well with our previous CARS microspectroscopic study of multi-lamellar vesicle (MLV). Owing to the high density of C-H bonds in the aliphatic chains, similar CARS signal was also observed on MLV at the C-H stretching vibrational mode [16]. As a result, we succeeded in vibrationally resonant imaging of an organelle in a living cell using multiplex CARS microspectroscopy.

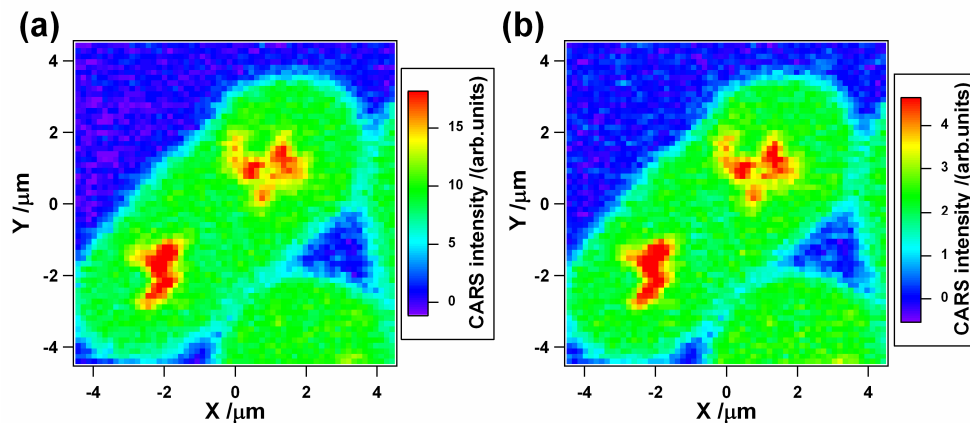


Fig. 3. Vibrationally resonant CARS imaging using the differentiation method (a) and a method using a conventional lineshape function described in Eq. (1) (b). Note that the contrast and signal-to-noise ratio is dramatically improved in comparison with Fig. 2(a).

The spectral profile of the CARS signal is often fitted by the following function [4, 11, 13, 25];

$$I(\omega) = \left| A_{\text{NR}} e^{i\phi} + \sum_{\text{R}} \frac{A_{\text{R}} \Gamma_{\text{R}}}{\Gamma_{\text{R}} - i(\omega - \Omega_{\text{R}})} \right|^2. \quad (1)$$

Here $I(\omega)$ is the observed signal intensity, A_{NR} and ϕ the amplitude and phase of the nonresonant background, A_{R} the amplitude of the Raman resonance signal, Ω_{R} the Raman frequency of the molecule, and Γ_{R} the dephasing rate of the Raman band. It is informative to

compare our method with the conventional analysis using Eq. (1). The spectral profile of the CARS signal in Fig. 1 is fitted by Eq. (1) in wavenumber region from 2588 to 3135 cm^{-1} . Here we assumed that the amplitude of the nonresonant background is described by a second-order polynomial function, and that only one Raman resonance is observed. The Raman frequency, dephasing rate, and phase of the nonresonant background, namely, Ω_R , Γ_R , and ϕ , are determined to be 2894 cm^{-1} , 69 cm^{-1} , and 1.8 radian, respectively. Since there are many fitting parameters, the values Ω_R , Γ_R , and ϕ are fixed in the fitting procedure for each spatial point. The resultant CARS image using the amplitude A_R in Eq. (1) is shown in Fig. 3(b). The original data is the same as that of Fig. 2. The CARS image in Fig. 3(b) is very similar to Fig. 3(a). It means that the vibrationally resonant CARS image can be extracted not only using the complicated lineshape function described in Eq. (1) but also using the simple differentiation technique demonstrated in the present paper.

4. Conclusion

In conclusion, vibrational imaging of a living yeast cell has been performed by supercontinuum-based multiplex CARS microspectroscopy. Owing to the broadband multiplex CARS detection, the spectral profile of the CARS signal can be analyzed in detail. The differentiation method enables us to extract only the resonant CARS image with the high vibrational contrast. The clear vibrational image of a yeast cell itself and mitochondria is successfully obtained. In comparison with the conventional fitting analysis, the differentiation technique is simple and sensitive, and is extremely useful in enhancing the vibrational contrast.

Acknowledgments

This research is supported by a Grant-in-Aid for Creative Scientific Research (No. 15GS0204) from the Ministry of Education, Culture, Sports, Science, and Technology of Japan. H. K. is supported by a Grant-in-Aid for Young Scientists (B) (No. 15750005) from Japan Society for the Promotion of Science, and research grants from The Kurata Memorial Hitachi Science and Technology Foundation. The authors thank Ms. Y. -S. Huang for her help in sample preparation and Dr. T. Karashima and Prof. M. Yamamoto for supplying us the strain of *S. pombe*.